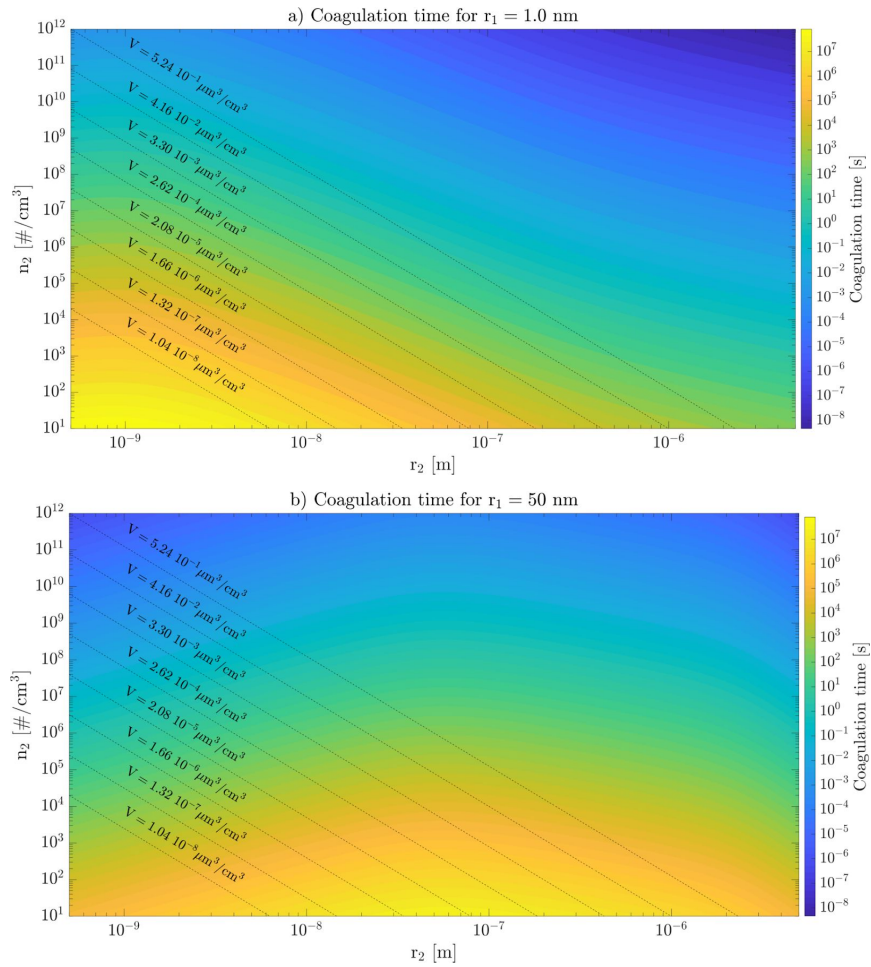


# Supplementary Information for “The role of plume-scale processes in long-term impacts of aircraft emissions”

Figure 1: Coagulation timescales for different number densities ( $n_2$ ) of the scavenging particles with a particle radius ( $r_2$ ). The scavenged particle has a radius  $r_1$ .



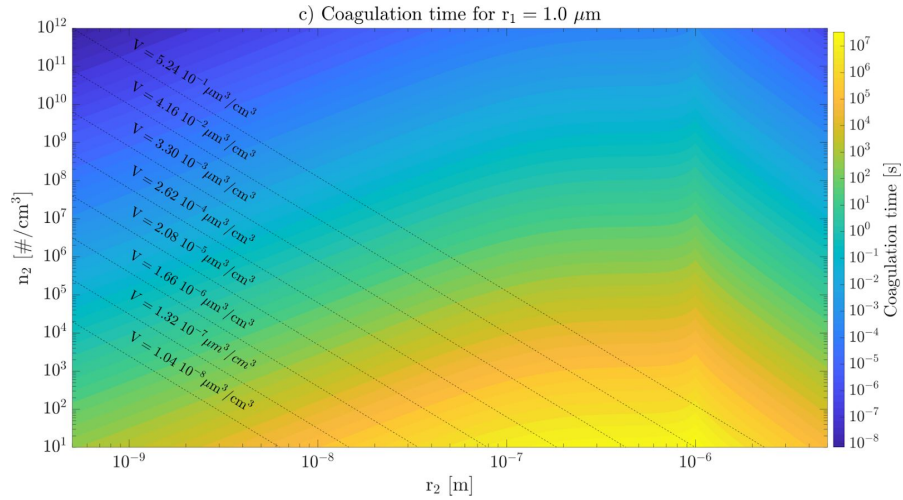
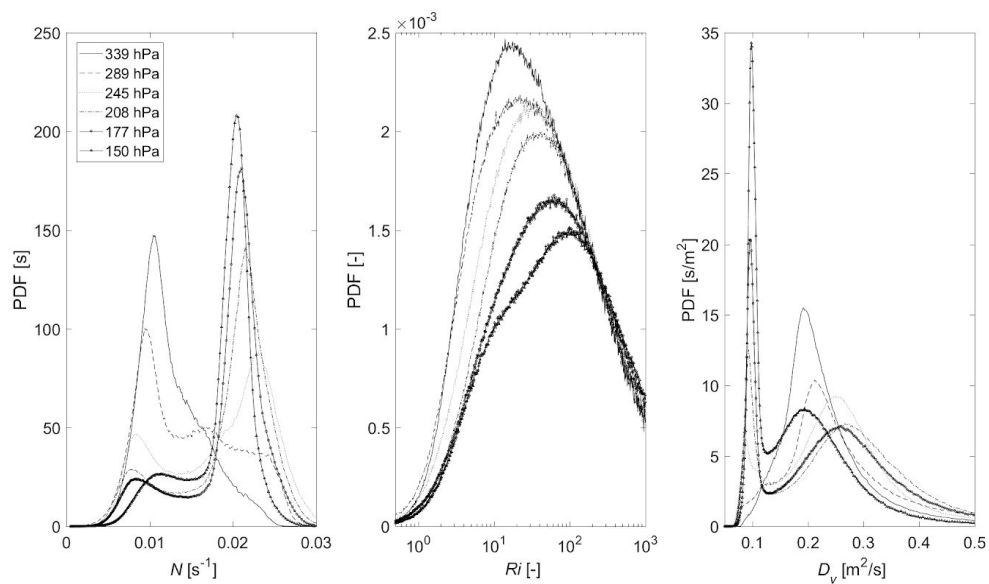
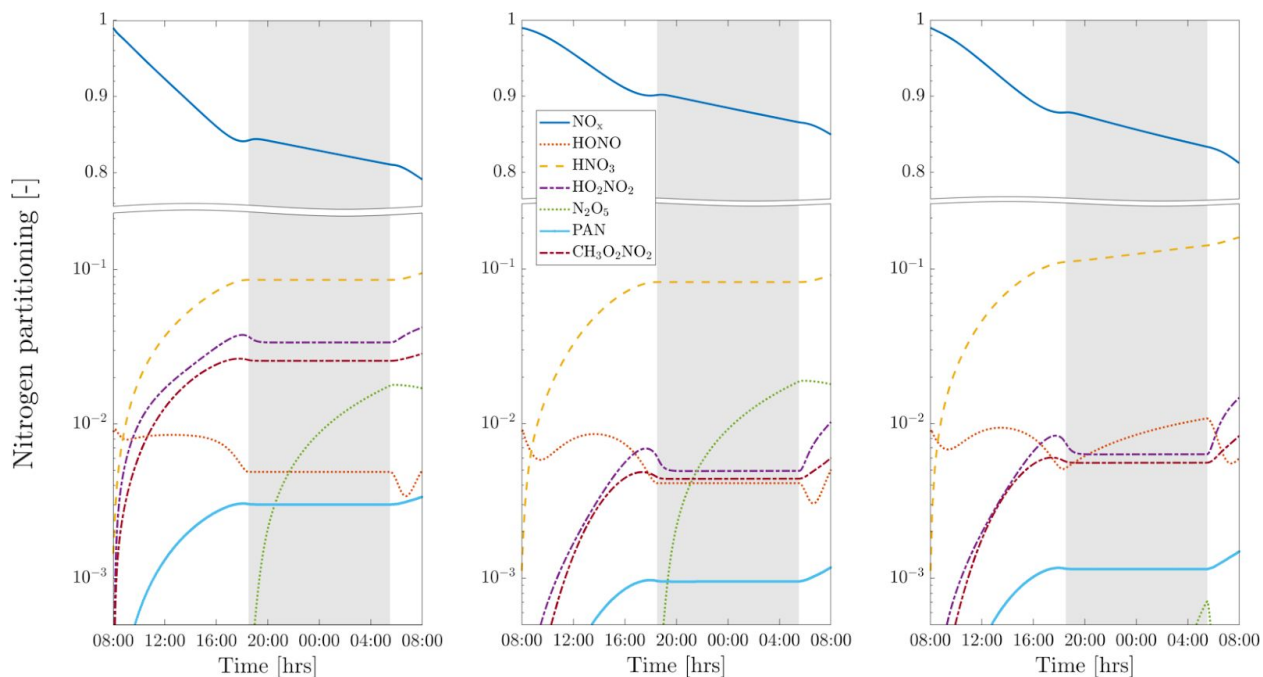


Figure 1 shows scavenging timescales as a function of the number densities and radius of the scavenging particles (particle 2) with different radius of the scavenged particle (particle 1). Timescales decrease with increasing difference between  $r_1$  and  $r_2$ .

**Figure 2: Probability distribution functions of the Brunt-Väisälä frequency, Richardson number, and vertical diffusion coefficient at different pressures obtained from the Modern-Era Retrospective analysis for Research and Applications, Version 2 (MERRA-2) dataset for the year 2015.**



**Figure 3: Partitioning of emitted nitrogen species as computed according to the instant dilution approach (left), the plume model in an ice subsaturated environment (middle) and in an ice supersaturated environment (right). Pressure and temperature are set to 240 hPa and 210 K respectively.**

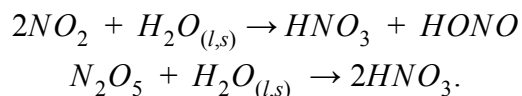


In addition to changes in the  $\text{NO}_x$  lifetime, we find that the partitioning of nitrogen between different species is significantly different between the instant dilution approach and APCEMM. Figure 3 shows the partitioning of emitted  $\text{NO}_x$  as a function of time for the two models. Results in an ice supersaturated environment are also displayed as heterogeneous chemistry on contrail ice crystals has a significant on the nitrogen partitioning.

For the ice subsaturated case, HONO and nighttime  $\text{N}_2\text{O}_5$  match with good precision between the instant dilution and the plume models. However, mixing ratios of  $\text{NO}_x$ ,  $\text{HO}_2\text{NO}_2$ , PAN and  $\text{CH}_3\text{O}_2\text{NO}_2$  are lower with APCEMM. The discrepancies do not reduce with time indicating that the instant dilution approach leads to a non-vanishing perturbation in the nitrogen partitioning which affects photochemistry, heterogeneous chemistry and aerosol formation.

The different results between the subsaturated and supersaturated cases are consequences of heterogeneous chemical reactions on the surface of ice crystals, which have a larger aerosol surface area, compared to soot or sulfate aerosols. The

differences between both simulations lie in the  $\text{NO}_x$ ,  $\text{HNO}_3$ , HONO and  $\text{N}_2\text{O}_5$  mixing ratios, which are direct consequences of the following heterogeneous reactions:



In an environment with a high relative humidity, heterogeneous chemistry leads to  $\text{NO}_x$  and  $\text{HO}_x$  sequestration. The production of  $\text{HNO}_3$  through  $\text{N}_2\text{O}_5$  hydrolysis leads to a larger fraction of  $\text{HNO}_3$  as a percentage of  $\text{NO}_y$ . In the subsaturated (resp. supersaturated) case, the fraction is 15.3% (resp. 25.4%). The instant dilution assumption predicts a  $\text{HNO}_3$  fraction of 14.8% in the subsaturated case. The nighttime behavior of HONO is also affected by heterogeneous depletion of  $\text{NO}_2$ . Halogen reservoir species do not play an important role in the nitrogen partitioning because of their relatively low abundance around the tropopause. Flying higher, in the stratosphere, could change this behavior.

**Figure 4: Contrail effective radius, extinction-weighted and horizontally-integrated. Only regions where the mean horizontally-integrated extinction is greater than  $10^{-6}$  are displayed. The vertical axis represents the distance with respect to the flight altitude after vortex sinking. The flight altitude before vortex sinking is at a pressure altitude of 10.6 km. Vortex sinking causes the plume to settle at a new altitude, 112 m lower, corresponding to the origin of the vertical axis. An upward velocity of  $5 \text{ cm s}^{-1}$ , a relative humidity of 108.0% and a temperature of 210 K are chosen.**

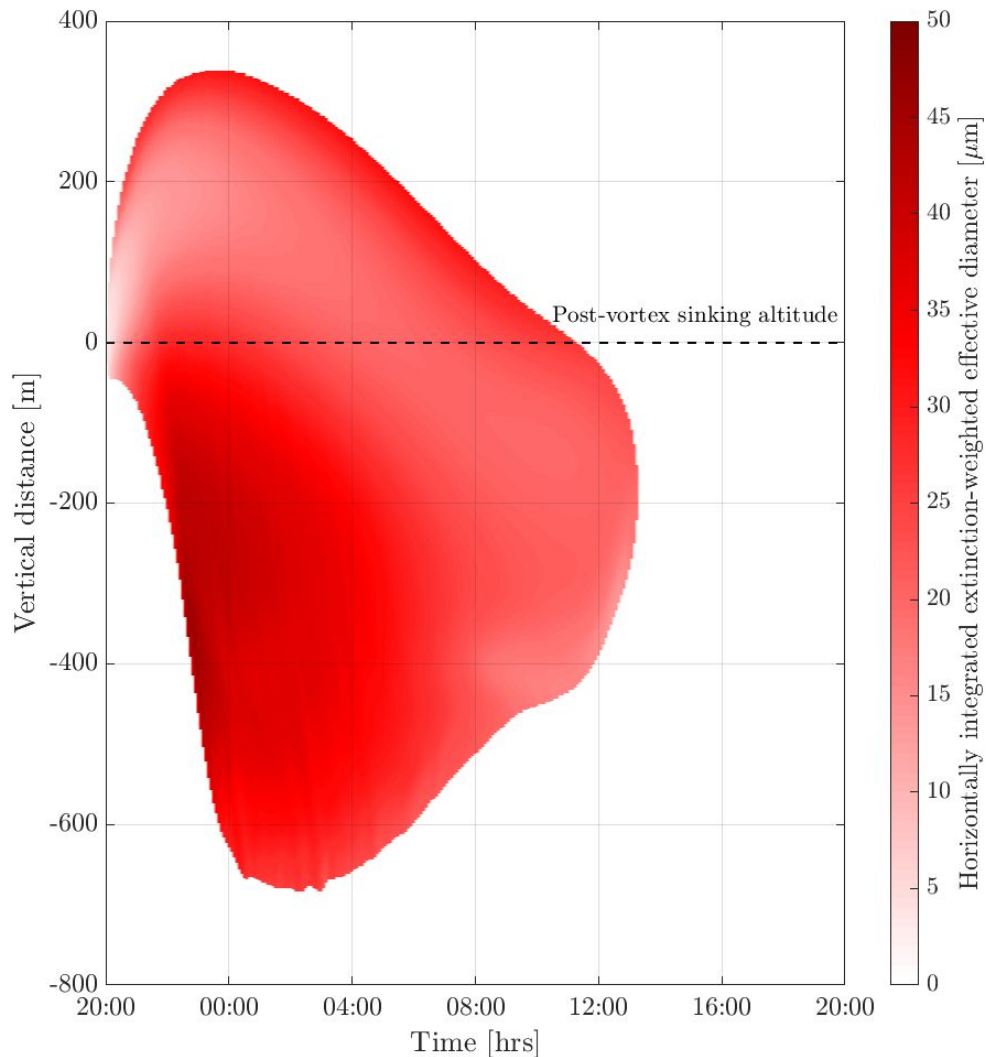
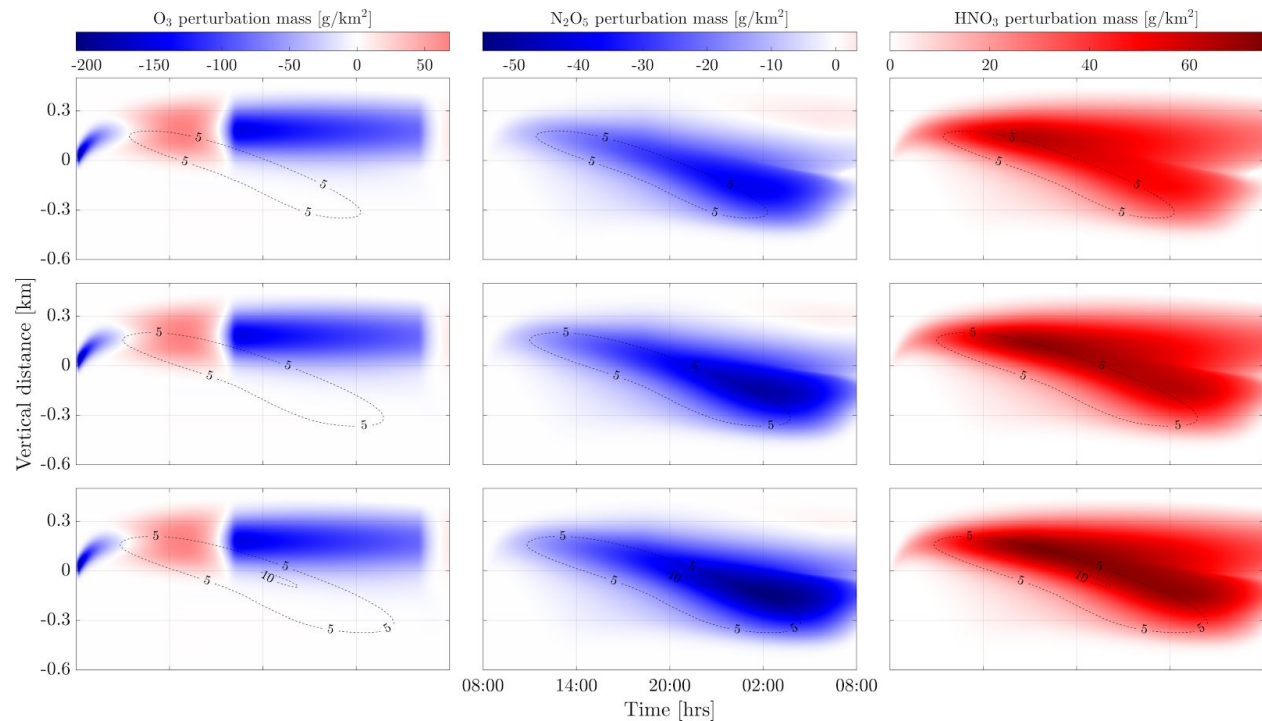


Figure 4 shows the contrail effective radius, weighted by extinction, integrated horizontally. Contrails consist of a core region where the relative humidity is close to 100% (because the mixing of supersaturated air happens on a timescale much greater than the timescale required for the ice crystals to grow) and an outer region, forming a fall-streak. Both of these regions have different microphysical properties. The core

consists of a large number density of ice crystals with a relatively low ice mass and an effective diameter of approximately 5-10  $\mu\text{m}$  while the edge of the contrail has a low number density but uptakes a large part of the surrounding water vapor, leading to a spatially non-uniform contrail ice mass.

Gravitational sedimentation causes larger crystals to fall more rapidly leading to a vertical layering of crystals with different sizes. Due to colder temperatures, ambient supersaturation on the upper side of the contrail enhances the ice crystal growth rate, and thus generates larger crystals.

**Figure 5: Contours of horizontally-integrated  $\text{O}_3$  (left),  $\text{N}_2\text{O}_5$  (center) and  $\text{HNO}_3$  (right) plume perturbations for different soot emission scenarios: 0.02 (top), 0.04 (middle), 0.06  $\text{g}/\text{kg}_{\text{fuel}}$  (bottom) respectively. Dashed lines show contours of the horizontal ice water path in  $\text{g}/\text{m}^2$ . Vortex sinking is applied prior to the simulation, such that the initial emission occurs at +112 m on the vertical axis. A wind shear of  $0.004 \text{ s}^{-1}$  is applied.**



In addition to changing the optical properties of the contrail, the soot emissions index affects the chemical impact of the plume. Figure 5 shows the evolution of several key chemical species over the contrail lifetime. Perturbations of  $\text{O}_3$ ,  $\text{N}_2\text{O}_5$ , and  $\text{HNO}_3$  are displayed for each scenario. The horizontal ice water path is also displayed, showing the location and extent of the contrail. Asymmetry in the vertical profiles arises because of gravitational settling of ice crystals and heterogeneous chemistry on their surface.